Characterization of Supported Cylinder–Planar Germanium Waveguide Sensors with Synchrotron Infrared Radiation

JITRAPORN VONGSVIVUT, JASON FERNANDEZ, SANONG EKGASIT, and MARK S. BRAIMAN*

Department of Chemistry, Faculty of Science, Chulalongkorn University, Bangkok 10330 Thailand (J.V., S.E.); and Chemistry Department, Syracuse University, Syracuse, New York 13244-4100 (J.F., M.S.B.)

Cylinder–planar Ge waveguides are being developed as evanescent-wave sensors for chemical microanalysis. The only non-planar surface is a cylinder section having a 300-mm radius of curvature. This confers a symmetric taper, allowing for direct coupling into and out of the waveguide's 1-mm² end faces while obtaining multiple reflections at the central <30-μm-thick sensing region. Ray-optic calculations indicate that the propagation angle at the central minimum has a strong nonlinear dependence on both angle and vertical position of the input ray. This results in rather inefficient coupling of input light into the off-axis modes that are most useful for evanescent-wave absorption spectroscopy. Mode-specific performance of the cylinder–planar waveguides has also been investigated experimentally. As compared to a blackbody source, the much greater brightness of synchrotron-generated infrared (IR) radiation allows a similar total energy throughput, but restricted to a smaller fraction of the allowed waveguide modes. However, such angle-selective excitation results in a strong oscillatory interference pattern in the transmission spectra. These spectral oscillations are the principal technical limitation on using synchrotron radiation to measure evanescent-wave absorption spectra with the thin waveguides.

Index Headings: **Tapered waveguides; Evanescent wave absorption spectroscopy; Synchrotron IR radiation; Blackbody IR source; Throughput.**

INTRODUCTION

Development of mid-infrared (MIR) waveguides fabricated from various IR-transparent materials has been driven by the goal of performing surface-sensitive chemical analysis. The general approach is known as attenuated total reflection (ATR) or evanescent-wave spectroscopy (EWS).[1] With this technique, the waveguide can be regarded as an internal reflection element (IRE) wherein the incident light experiences total internal reflection at the interface between media of different refractive indices. At each reflection, the evanescent wave penetrates a fraction of wavelength beyond the high-index waveguide into the lower-index medium (i.e., the sample). The penetration depth of the evanescent wave is typically in the range of 0.5–5 μm for MIR light propagating through useful IREs. As a consequence, only a thin layer of the sample is probed.

The detection limit of ATR spectroscopy is as yet insufficient for it to be considered generally suitable as a trace method. Hence, there is substantial interest in novel methods for improving the surface sensitivity of MIR waveguides. One approach, for both fiber optics and planar waveguides, has been to reduce the cross-sectional area of the sensor. This tends to increase the fraction of the total energy carried in the evanescent wave, but has the limitation of reducing the optical power available for detection.

The greatest achievements in developing chemical sensors for tiny samples have been carried out with silica-based fibers and planar waveguides, which are useful in the near-infrared (NIR) spectral region.[2–4] However, much useful chemical information is lost due to the opacity of silica composites in the MIR spectral range (i.e., 400–4000 cm^{-1}), where specific molecular fundamental vibrational fingerprints are more readily interpreted, compared to the overtone and combination bands at NIR frequencies.

We have instead focused on single-crystal germanium (Ge) as an IRE for the MIR region because of its relatively low cost, its transparency from 5000–800 cm^{-1}, and its high refractive index (4.0), as well as its excellent chemical and biochemical inertness. A significant drawback of Ge is its brittleness and relatively low mechanical strength, leading to significant challenges in fabrication. However, several types of thin planar Ge waveguides under 50 μm in thickness have now successfully been fabricated and applied in EWS analysis of sub-μL volatile liquids, ng-quantity thin films, coatings on fibrous samples, and single- and multilayer biological membranes covering small (<1 mm^2) areas.[5–12] These studies demonstrated a significant improvement in sensitivity for such small samples as a result of the larger number of internal reflections per unit length.

Most recently, the development of tapered cylinder–planar Ge waveguides has simplified the coupling of broadband IR light from the blackbody source of commercial FT-IR spectrometers into the waveguide.[10–12] These waveguides are designated as cylinder–planar because while one surface is planar, the other is ground and polished as a cylinder surface, resulting in a gradual, symmetrical taper away from the central minimum in thickness (see Fig. 1). The larger cross-sectional area at the ends of the waveguides makes it easy to align them with respect to both the focused IR beam and the detector, eliminating the need for an IR microscope and permitting the use of the waveguides in a horizontal configuration, the most useful for typical sensing applications.[12]

However, these thin tapered Ge waveguides have in practice not afforded as high a spectral signal-to-noise (S/N) ratio in observed broadband FT-IR spectra as was predicted theoretically by using standard approximations and simplifying assumptions in order to predict the range of modes that would be excited.[5] In the current work, the

Received 21 August 2003; accepted 2 October 2003.

* Author to whom correspondence should be sent. E-mail: mbraiman@syr.edu.

0003-7028/04/5802-0143$2.00/0

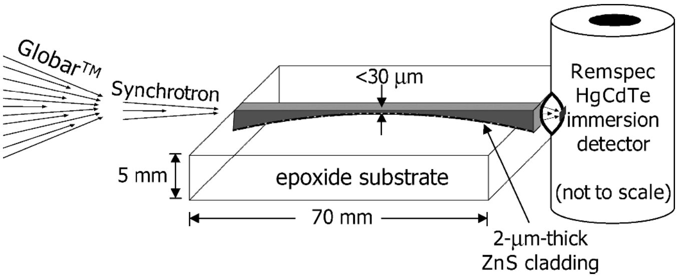

FIG. 1. Schematic configuration of cylinder–planar tapered Ge waveguide used as a miniature evanescent-wave sensor. The waveguide is mechanically supported by a cast epoxide substrate. The top flat surface near the <30-μm-thick central region of the waveguide is the sensing area. The bottom surface of the waveguide is a cylindrical sector with a radius of 300 mm, coated with a 2-μm-thick ZnS cladding layer. Incident light indicated at left is generated from a broadband IR source, either a standard blackbody (Globar™) internal to the spectrometer, or an external synchrotron (U2B beamline at NSLS, Brookhaven National Laboratory). A liquid-N_2-cooled HgCdTe immersion detector, placed as close as possible to the exit end of the waveguide, is used to measure the transmitted IR radiation.

reasons for the discrepancy between the theoretical and observed performances have been investigated in more detail, both with calculations and by using broadband synchrotron IR radiation to carry out mode-specific measurements.

Our original hope was that a combination of synchrotron-based IR spectroscopy with the symmetrically tapered <30-μm-thick Ge waveguides would create a new opportunity for analyzing tiny samples with improved spectral quality. This goal has not yet been realized due to the strong interference patterns produced by combining highly spatially coherent synchrotron light with thin waveguides. Nevertheless, the results with the synchrotron radiation lead to useful conclusions that are likely to result in improved designs for MIR waveguide sensors.

EXPERIMENTAL

Waveguide Fabrication. Fabrication of cylinder–planar tapered waveguides was carried out as described previously.[12] In brief, a 70-mm-diameter, 3-mm-thick single-crystalline Ge disk was first cylindrically ground and polished to a 600-mm-diameter curvature at a commercial optical polishing house (K & S Optics, Binghamton, NY), producing a curved surface on one side of the disk (see Fig. 1). The curved surface was then coated with a 2-μm-thick ZnS cladding layer using chemical vapor deposition. The ZnS-coated Ge disk was diced into 2-mm-wide strips, and the parallel-diced sides were ground to give a final width of 1–1.5 mm. A single Ge strip was embedded into an ~1-cm-thick epoxide substrate by casting it, planar-side down, into the freshly mixed resin and hardener (Buehler Ltd., Lake Bluff, IL). The minimum thickness of the waveguide was subsequently reduced from its initial value (~2 mm) down to the final tapered thicknesses of <30 μm, by grinding and polishing its exposed flat surface. Towards the end of this process, the thickness was periodically measured by using the interference pattern appearing on the reflectance spectrum[13] obtained with the IR beam perpendicular to the waveguide's planar (flat) surface. This reflectance spectrum was obtained by using an IR microscope (IR-Plan Infrared Microscope Accessory, Spectra-Tech, Stamford, CT) coupled to an FT-IR spectrometer (Midac Illuminator) operating with 1-cm^{-1} resolution and 256 scans.

Optical Alignment and Conditions for Spectral Data Collection. Figure 1 shows schematically the optical configuration of the cylinder–planar Ge waveguide with respect to the IR source and detector. The large differences in refractive indices enable the thin Ge layer (n_{Ge} = 4.0), sandwiched between ZnS cladding (n_{ZnS} = 2.2) and air (n_{air} = 1.0) or sample (e.g., water, n_{H_2O} = 1.34), to serve as a waveguide for MIR light.

Two different FT-IR spectrometers equipped with different IR sources were employed for spectral collections with the same cylinder–planar Ge waveguide in order to determine how the waveguide functions under different throughput conditions. The first was a Bruker IFS66 FT-IR spectrometer with the standard internal Globar™ source. The second was a Nicolet 860 FT-IR spectrometer interfaced with a synchrotron light source (U2B Beamline at National Synchrotron Light Source, Brookhaven National Laboratory). The latter spectrometer was additionally equipped with a standard internal Globar™ source that could be selected by switching a single computer-controlled mirror.

With both spectrometers, it was possible to configure the optical system to allow use of the tapered Ge waveguide either outside the spectrometer (i.e., via the external output port) or inside the main sample compartment as a traditional ATR accessory. For the out-of-compartment setup, the incident light exiting the external output port of the spectrometer was simply focused onto the entrance end of the waveguide by using a single off-axis paraboloid mirror with a 19.1-mm focal length (Melles Griot, Irvine, CA). Alternatively, several mirrors could be utilized inside the sample compartment of the spectrometer in order to focus the light onto the input end of the waveguide.

With either in-compartment or out-of-compartment setup, a liquid-N_2-cooled HgCdTe immersion detector (MOD-O2S1, Remspec Corp., Sturbridge, MA), with an active area of 0.50 × 0.50 mm^2 and D^* (10 kHz) ≥ 4 × 10^{10} cm Hz$^{1/2}$ W^{-1}, was mounted with its window directly against the output end of the waveguide. For some experiments investigating mode-specific behavior, an alternative immersion detector (FTIR-M16-0.10, Graseby Infrared), with an active area of 0.15 × 0.15 mm^2 and similar D^*, was utilized. The detector's angle was always fixed perpendicular to the top and side surfaces of the waveguide (i.e., the immersion lens optical axis was parallel to the waveguide axis), while its position was adjusted both horizontally and vertically to maximize the measured throughput of broadband IR light.

The same spectrometer parameters were utilized in comparisons between measurements with the standard Globar™ source and those with synchrotron IR radiation. All spectra shown below were acquired at a gain of 1, resolution of 8 cm^{-1}, and measurement bandwidth of 7800 cm^{-1}. The moving mirror of the interferometer had its optical retardation velocity set to give a modulation frequency of 100 kHz for the HeNe reference beam. The coadded scan time was 5 min for all measurements. Mertz phase correction and zero-filling of 2 were set as default acquisition parameters. Happ–Genzel and Black-

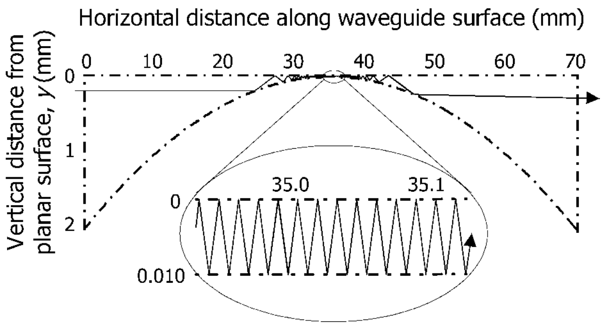

FIG. 2. Typical calculated reflection pattern of a light ray propagating through a symmetrically tapered cylinder–planar waveguide with a total length of 70 mm, a circular radius of 300 mm for the cylinder surface, and a minimum thickness t of 10 μm. This particular ray was assumed to impinge perpendicular onto the waveguide's ~2-mm-high entrance face ($\theta = 0°$), at a distance y of 0.20 mm from the flat surface. This results in this ray's propagation through the thinnest part of the waveguide near the critical angle for total internal reflection at a Ge–ZnS interface. Note that the exaggerated vertical scale in both the main figure and the inset results in distorted apparent reflection angles.

man–Harris three-term apodization functions were applied for Nicolet and Bruker instruments, respectively.

Ray-Tracing Calculations. We traced a series of input rays impinging on the end of the waveguide through its entire length. This required calculating many reflections (typically several hundreds) for each input ray. The analytical geometry required is rather simple, but solution of this type of problem (multiple internal reflections between a planar and cylinder surface) is not included in commercial ray-tracing programs. Therefore, we wrote our own program using MATLAB® (The Mathworks Inc., Natick, MA, version 5.3.1).

We simplified the problem by limiting ourselves to two dimensions. The trajectories of all incoming rays are assumed to be confined to a plane that is perpendicular to the waveguide's upper planar surface as well as to the (axis of) the lower cylinder surface. The traced rays that are restricted to this plane are then calculated as a series of reflections from a line and a circular arc (see Fig. 2). Each input ray, impinging on the end of the waveguide at angle θ with respect to the waveguide axis and at a depth y below the planar surface, first has its refraction angle θ' into the high-index waveguide calculated according to Snell's law. The program then propagates the ray (by setting the reflected angle equal to the incident angle at each internal reflection point) until it reaches the exit end of the waveguide or else exceeds the critical angle for reflection from the upper or lower surfaces. Our program reduces the problem to a very elementary treatment with ray optics, omitting features (such as the displacement of the reflected ray along the dielectric boundary) that have been shown to be required for a more accurate treatment of the ray-tracing problem for a multi-reflection waveguide. The main output of the routine is the maximum sensing angle φ achieved inside the waveguide for each pair of input parameters (y, θ). One of the additional inputs required for the program is a subroutine defining the height and slope of the lower curved surface as a function of horizontal distance from the center of the waveguide. In the present work, this subroutine was set to define only a circular arc in order to compare results with those obtained by experiments, but it could alternatively be set to other functional forms of curves of interest. Almost any differentiable function gives accurate ray-trace calculations with the routines, as long as the function is sufficiently smooth (i.e., having no point with a radius of curvature less than ~2 mm).

RESULTS AND DISCUSSION

We have recently reported a substantial improvement in sensitivity achieved by symmetrically tapering Ge waveguide evanescent-wave sensors and decreasing their central thickness to 7–15 μm.[12] Absorption intensities of spectra acquired with thinner waveguides are enhanced as an inverse function of the waveguide thickness raised to a power greater than 1, due to increases both in the number of internal reflections per unit length and in the amount of electromagnetic energy contained within the evanescent wave at each reflection. Tapering also simplifies the optical alignment since only common focusing optics (off-axis paraboloid mirrors) are needed. As a result, spectral absorption measurements on even tiny (nanogram) samples are simple and quick.

Nevertheless, the absorption intensities observed[12] corresponded only to those expected for 3–5 reflections, rather than >25 reflections expected for a 20-μm-thick waveguide with an average internal propagation angle of 45° and a sensing length of ~1–2 mm. In an attempt to evaluate how light focused onto the end of the waveguide is coupled into modes with varying propagation angles, we have performed both ray-tracing calculations and measurements at selected angles using the highly collimated broadband light available from a synchrotron.

Ray Tracing of Cylinder–Planar Waveguides. A typical traced ray is shown in Fig. 2 for a cylinder–planar Ge waveguide with a total length of 70, an entrance/exit height ratio of 1 (i.e., symmetrical tapering), and a minimum thickness of 0.010. This corresponds to a circular radius of 300. These dimensions (assuming units of mm) match quite closely to those of the physically realized waveguides that we have utilized for evanescent-wave sensing measurements. Note that the vertical scale in Fig. 2 is greatly exaggerated relative to the horizontal scale. This creates the illusion that wherever the curved waveguide surface is sloped (i.e., non-horizontal), the incident and reflection angles are unequal.

Near the center of the waveguide, the particular ray shown in Fig. 2 propagates very close to the critical off-axis angle of $\varphi = 56.6°$ for propagation of light through a ZnS-clad Ge waveguide, ($n_{21} = 2.2/4.0$). For this critical ray, there are a very large number of internal reflections (133 per mm of travel; 67 per mm for only the sensing surface) at the thinnest central sensing region, as shown in the expansion (inset) of the centermost 0.1 mm of the waveguide. At $x = 0$ (i.e., the entrance end of the waveguide), this ray has a y value of 0.2 mm and an initial angle inside the waveguide of $\theta' = 0°$. Using Snell's law ($n_{Ge} \sin \theta' = n_{air} \sin \theta$), this also corresponds to an impinging angle of $\theta = 0°$ (i.e., perpendicular to the entrance face) for the ray propagating in air prior to entering the waveguide.

Figure 3 shows the variation of number of total internal reflections within the 0.010-mm-thick waveguide as a function of y, holding the impinging angle θ constant at

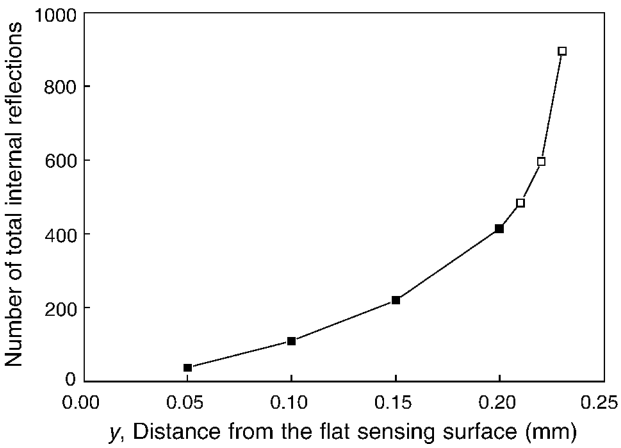

FIG. 3. Plot of the calculated number of total internal reflections vs. vertical distance (y) of the impinging ray from the upper planar surface of a 70-mm-long, symmetrically-tapered, cylinder–planar waveguide with a minimum thickness of 10 μm. The light ray is assumed to enter the waveguide on-axis ($\theta = 0°$). Values of y above 0.20 mm (□) give reflections that exceed the critical angle for a Ge–ZnS interface. Therefore, the maximum number of total internal reflections in a ZnS-clad Ge waveguide of these dimensions is approximately 400, and is achieved at $y = 0.20$ mm.

0°. There is a substantial increase in number of total internal reflections as y is increased. However, propagation via total internal reflection is allowed only for $y \leq 0.20$ mm, i.e., only for rays entering the waveguide along the 10% of its entrance face closest to the planar surface. For an on-axis ray entering farther than this from the waveguide's flat surface, the propagation angle exceeds the critical angle for a Ge–ZnS interface before the ray reaches the center of the waveguide. As a consequence, for $\theta = 0°$, only light rays entering within 0.20 mm of the flat surface contribute to the detected light. At this y value, the number of total internal reflections in the model waveguide described is ~400, and this turns out to be (approximately) the maximum number of internal reflections allowed for this tapered waveguide at any combination of y and θ.

By calculating ray-traces such as those in Fig. 2 while varying both θ and y, it was possible to determine all possible combinations of these two parameters for which light can propagate through a particular waveguide. For each of the allowed rays, the ray-trace program also provided the sensing angle $\varphi(\theta, y)$, which is the maximum angle that the ray makes with respect to the planar surface of the waveguide at the thinnest (sensing) portion of the waveguide. These results are shown schematically in Fig. 4 for various thicknesses of the cylinder–planar waveguide (including several that match those used in experimental measurements). As expected, with decreasing waveguide thickness there is a corresponding decrease in the range of allowed (θ, y) pairs, corresponding to a decrease in total throughput. However, there is also the evolution of fascinating structure in the contour plots as the waveguides get thinner, including the gradual pinching-off of isolated "islands" at very specific combinations of θ and y and the clear appearance of a thumb-like protrusion that indicates a large throughput allowed for light entering the waveguide from a specific angle just above 0°. We speculate that these regions may be mathematical "attractors", and therefore signs of chaotic (or near-chaotic) behavior for rays reflecting from such closely apposed non-parallel surfaces.

The optical invariant (one-dimensional version of the étendue) of a cylinder–planar waveguide in the vertical direction is normally calculated as the product of the numerical aperture (NA) and the thickness t. For a simple planar waveguide, this is equal to $t\sqrt{n_1^2 - n_2^2}$, where n_1 and n_2 are the refractive indices of the waveguide and cladding materials, respectively. In more general terms, and in particular at the entrance end of the waveguide, the optical invariant should be given by the following integral over the thickness t of the waveguide:

$$\text{étendue} = \frac{1}{2}\cdot\left\{\int_0^{t=2\,\text{mm}}\left[\int_{\theta_{\min}(y)}^{\theta_{\max}(y)}\cos\theta\, d\theta\right]dy\right\} \qquad (1)$$

In this formula, θ_{max} and θ_{min} are the extreme values of θ that can successfully propagate through the entire waveguide from a vertical position y within a cross-section at a specific horizontal position x where the optical invariant is being calculated, in this case, at the entrance of the waveguide. The refractive index n should in most generality appear inside the integral, but it is assumed in Eq. 1 to be 1.0 at the entrance of the waveguide, which faces air. (It can readily be seen that if all entering rays in a range of $\pm\psi$ are allowed to propagate through a waveguide of constant thickness t, this formula gives étendue $= t \sin\psi$, i.e., the thickness times the numerical aperture, as it should.)

Using Eq. 1 and setting the integral limits according to the allowed rays from the ray-tracing calculations, the étendue value for the 0.014-mm-thick Ge waveguide for the data matrix in Fig. 4 is 0.0510 mm (~51.0 μm). This is remarkably close to that given by the simple formula for planar waveguides (étendue $= t\sqrt{n_1^2 - n_2^2}$), which gives the value of 46.7 μm. The closeness of the two values suggests that light illuminating the end face uniformly and then propagating to the center of the waveguide could be accurately represented as a bundle of rays filling the numerical aperture of 3.3 (i.e., according to the formula NA $= \sqrt{n_{Ge}^2 - n_{ZnS}^2} = \sqrt{(4.0)^2 - (2.26)^2}$ for a Ge–ZnS interface), at uniform density.

However, the hypothesis that the numerical aperture of the sensing region of the waveguide gets filled uniformly is contradicted by a more careful analysis, which shows that the distribution of intensity as a function of angle is far from uniform (Fig. 4). In particular, rays that approach close to the critical angle (red-green colors) are somewhat under-represented. This is undesirable behavior for an evanescent-wave sensor, because the on-axis rays undergo relatively few internal reflections and have a lower evanescent-wave electric-field strength than rays near the critical angle. Unfortunately, it is completely consistent with the experimental results on the cylinder–planar waveguides, which show substantially lower evanescent-wave absorption intensities than would be predicted for modes evenly distributed over all the "allowed" angles for the cylinder–planar sensing region at the center of the waveguide[12] (see below).

It is of interest to consider how changes in the shape of the waveguide might affect this result. In particular, we examined how it depends on the curvature radius R

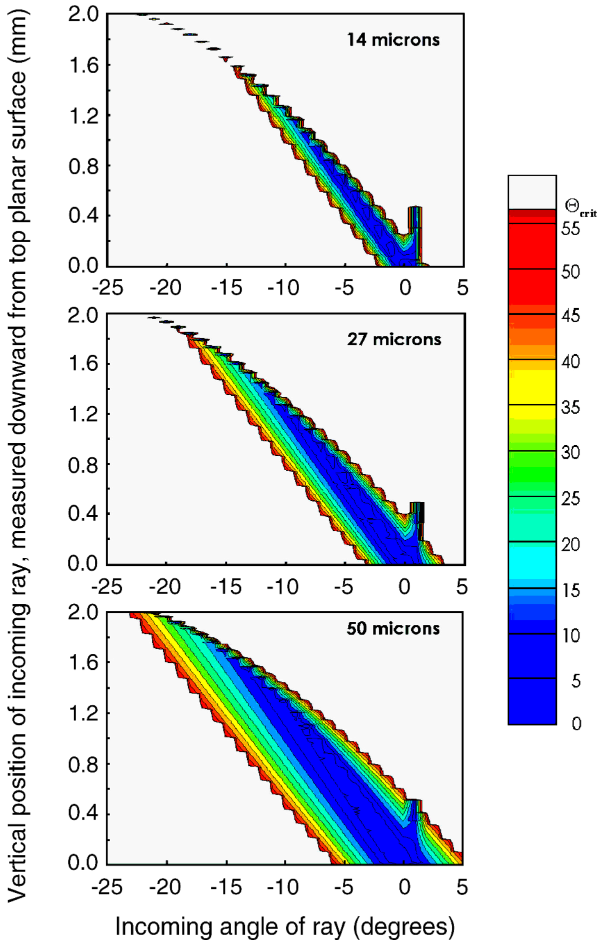

FIG. 4. Summary of results of 10 251 ray-trace calculations on each of three different cylinder–planar waveguide sensors, all having a circular radius of 300 mm but different minimum thicknesses (14, 27, and 50 μm) as indicated. These contour plots show on the horizontal and vertical axes the initial conditions for each calculated ray (respectively, θ, the entrance angle in air prior to entering into the waveguide; and *y*, the distance measured downward from the top planar surface). The *z*-axis corresponds to the maximum angle φ at which the ray is calculated to propagate in the thinnest (sensing) region of the waveguide. Contours are given at 5° intervals. The *z*-levels are also color-coded according to the key at right, with gray indicating all initial conditions that result in the ray exceeding φ_{crit} = arccos(2.2/4) for a Ge/ZnS interface of the waveguide.

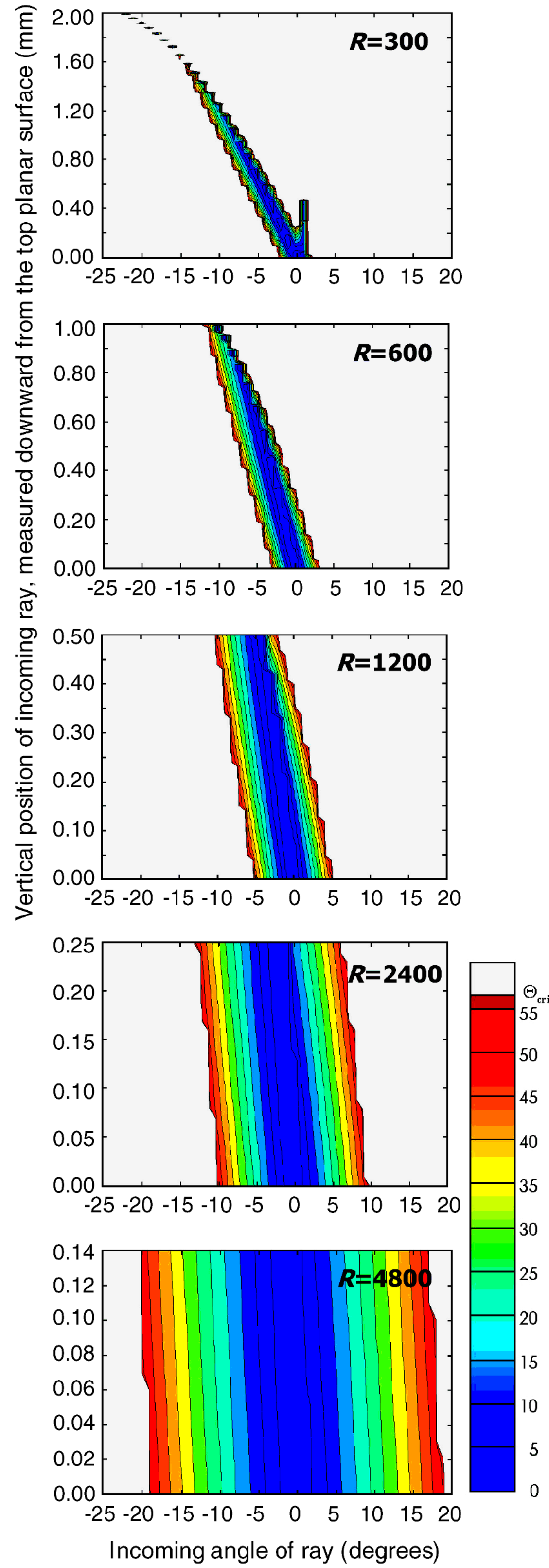

FIG. 5. Sensing-angle plots for rays impinging on the entrance faces of 14-μm-thick cylinder–planar waveguides with different values of circular radius *R* (300, 600, 1200, 2400, and 4800 mm) as indicated. A larger radius of curvature results in thinner end faces, as indicated by the correspondingly smaller range for the *y*-axis scale. As in Fig. 4, *z*-axis contours are always calculated at 5° intervals. The color bar shown at right is applicable to all plots.

of the cylindrical bottom surface, at a constant waveguide center thickness *t* of 14 μm. We hoped this might provide some useful clues for improving the waveguide's performance. Figure 5 presents contour plots of cylinder–planar waveguides having the same length (70 mm) and center thickness (14 μm) as the top plot in Fig. 4, but with various values of *R*. Figure 6 presents a summary of calculations of the étendue of these waveguides. Although increasing *R* results in a reduction of the end heights of the 70-mm-long waveguides, our calculation indicates that waveguides with *R* values in a range of 1200–2500 show only a small decrease in throughput relative to that for *R* = 300 mm. In addition, a wider range of incoming angles with allowed sensing angles, achieved by a waveguide with a larger radius of curvature, leads to excitation of the far-off-axis modes in the sensing region of the tapered waveguide, the modes that are in fact useful for evanescent-wave absorptions. Thus we can in theory ob-

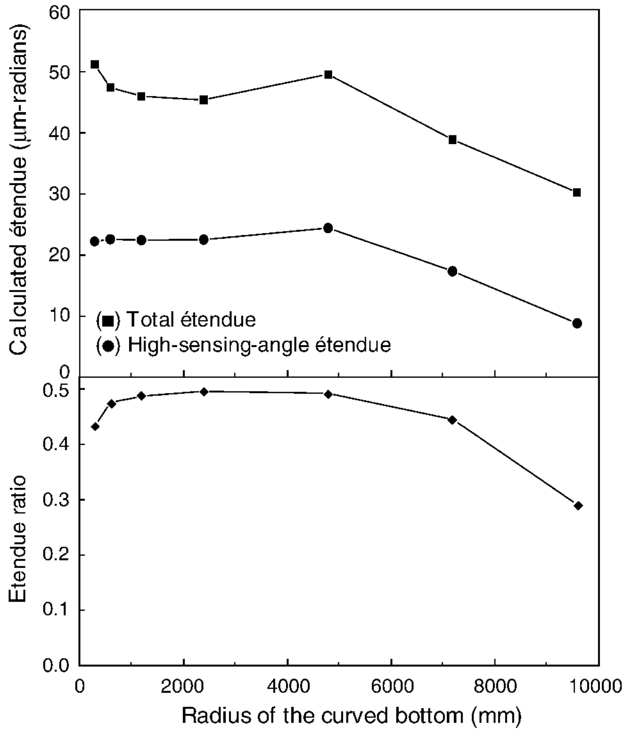

FIG. 6. (***Upper***) Plot of calculated total étendue (■) and high-sensing-angle étendue (●) of a 14-μm-thick cylinder–planar waveguide vs. curvature radius R of the bottom cylinder surface. Each value of total étendue was calculated from Eq. 1 (see text), taking appropriate limits for the double integral from the data matrix that gave the corresponding plot in Fig. 5. Because $\cos\theta \approx 1$ for most of the allowed input rays, each calculated étendue roughly equals the total colored (non-gray) area of the plot in Fig. 5. For the high-sensing-angle étendue, on the other hand, the range of the double integral was limited to just those plotted elements that correspond to sensing angles in the range of 25° to the critical angle (56.6°), giving roughly the green-to-red area of each plot in Fig. 5. (***Lower***) Ratio of the high-sensing-angle étendue to the total étendue as a function of the curvature radius R, based on plots in the upper part of the figure.

tain a significant improvement in the waveguide performance, simply by increasing the circular radius of the waveguide's curved bottom.

In order to investigate how the total étendue varies with R values, we performed étendue calculations, based on Eq. 1, on the entire data matrix of individual waveguides at different radii of curvature, which correspond to those contours in Fig. 5. The calculated total étendue are represented by (■) in Fig. 6. The plot shows the largest total étendue at the smallest R value (300 mm) as a result of the largest entrance aperture (2 mm^2) into the waveguide. In fact, it is impressive that the calculated étendue for all the R values indeed end up being so close to each other because this is a clear demonstration of the validity of the étendue as an optical constant. However, the étendue is not monotonic with R: it rises again at $R = 4800$ mm and drastically goes down afterwards.

In addition, we determined the fraction of the étendue associated with light rays that propagate at high angles in the sensing area. Therefore, a filter based on maximum sensing angle was applied to the data matrices in order to exclude those elements containing sensing angles less than an arbitrary angle (i.e., 25° for the present work) from calculation. The result of high-sensing-angle étendue, as shown in Fig. 6 (●), approaches the maximum theoretical value at $R = 4800$ mm, instead of the value of $R = 300$ mm obtained by the full calculation without filtering the data matrix. By ratioing the high-sensing-angle étendue to the total étendue, the lower curve (♦) in the same figure reveals waveguide sensors have optimum performance at a radius of curvature in a range of 2000–3000 mm, rather than the 300-mm-radius waveguide sensor used in practical measurements, for two reasons: (1) somewhat higher fractional throughput for higher-sensing angles, i.e., above 25°, with no loss of total throughput; and (2) an ability to selectively excite modes with high sensing angles by illuminating the end face of the waveguide with off-axis rays. By comparison, the calculations show that there is little or no selective excitation possible with the 300-mm-radius waveguide, in contrast to the contour lines of the 4800-mm-radius waveguide, which are almost perfectly vertical. This suggests that we could obtain exclusive light propagation with sensing angles greater than 25° by limiting input angles to be larger than 10°. As a consequence, the sensitivity of the waveguide should be significantly improved.

Throughput Measurements with Synchrotron Radiation. Figure 7 compares single-beam spectra of symmetrically tapered 14- and 27-μm-thick Ge waveguides obtained both with synchrotron IR radiation and with a standard blackbody (Globar™) source. For the synchrotron beam, the optics were aligned in two different setups along with the Nicolet 860 FT-IR spectrometer: (1) using the external output port with an out-of-compartment set-up; or (2) with the Remspec immersion detector and waveguide both mounted inside the internal sample compartment. The results demonstrate that the synchrotron radiation does not exceed the numerical aperture of the waveguides, because the detected throughputs are independent of waveguide thickness. As expected, the small effective source size of the synchrotron can totally pass through the minimum 46-μm étendue of the 14-μm-thick waveguide. The calculated one-dimensional étendue of the output of the U2B beamline at the National Synchrotron Light Source is far below 46 μm; in fact, it is somewhat under 0.1 μm, based on the published VUV parameters at NSLS as of December 2002.[14]

The results in Fig. 7 show that indeed there is a higher total energy throughput when using the synchrotron radiation, as compared to a blackbody Globar™ source, for both 14- and 27-μm-thick waveguides. For the thicker (27-μm-thick) waveguide, the increase in throughput intensity for the synchrotron, relative to the Globar™, is significant only above 2500 cm^{-1} (and up to 5000 cm^{-1} where the cutoff due to the Ge bandgap blocks all transmission in either case). In contrast, for the 14-μm-thick waveguide, the synchrotron affords higher throughput over all MIR frequencies.

Therefore, using synchrotron radiation can clearly help to increase the total light energy throughput with such thin waveguides. Furthermore, the use of synchrotron IR radiation allows a simple in-compartment set-up configuration using only flat mirrors, with no loss of energy. This is because the ~100-mm-focal-length mirror that the spectrometer uses to focus the beam into the sample com-

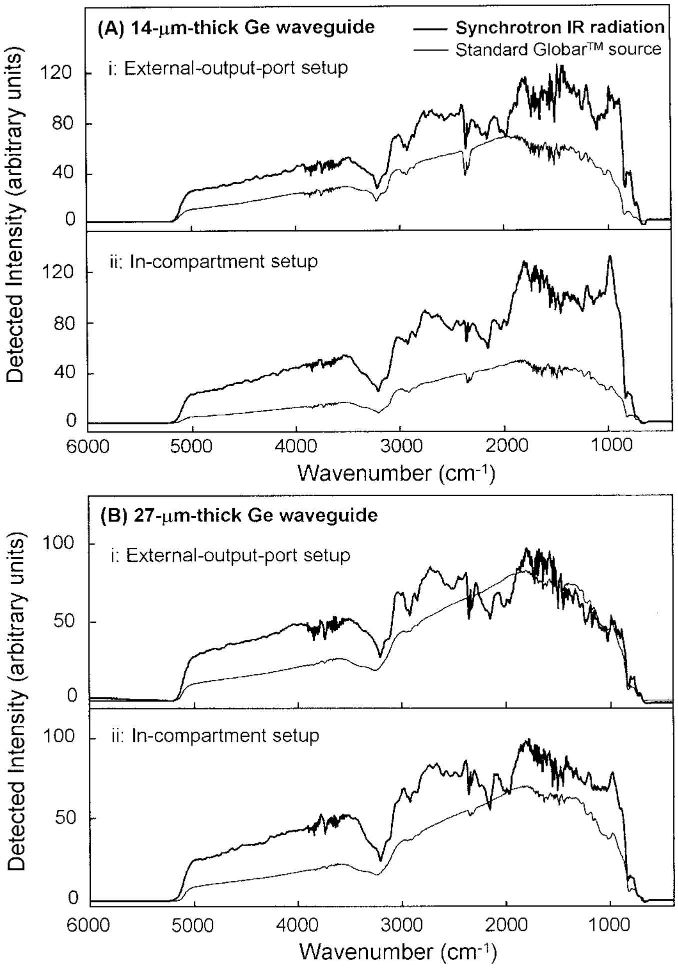

FIG. 7. FT-IR single-beam spectra of (**A**) a 14-μm-thick and (**B**) a 27-μm-thick Ge waveguide observed with synchrotron IR radiation, compared to those observed with a standard blackbody (Globar™) source. With each waveguide thickness, two different on-axis setups were examined: (***i***) using the external output port; and (***ii***) using the internal sample compartment. Throughput in each case was maximized by shifting the relative horizontal and vertical positions of the IR beam, waveguide, and detector.

partment is adequate to focus the highly collimated synchrotron beam into the ~1-mm^2 end of the waveguide. On the other hand, it can only focus a small portion of the Globar™ intensity into such a minute aperture.

Angle Dependence of Throughput and Absorbance Signals with Synchrotron Radiation. We measured the total synchrotron-generated IR energy throughput of the 27-μm-thick waveguide and the water absorbance signal at 3400 cm^{-1} for a standard 1-mm-diameter droplet of water as a function of the external incident angle θ. However, the results showed great variability. The ray-trace calculations in Fig. 4 help to explain this. They show that at any value of θ, widely different results can be expected depending on other aspects of the optical alignment of the waveguide relative to the synchrotron beam, specifically, entrance height y on the waveguide end face and the relative vertical displacement of the output end of the waveguide and the detector's immersion lens. At the time that measurements were made at the synchrotron (prior to performing the ray-trace calculations), we did not suspect such a strong dependence of throughput and absorbance signal on these beam height parameters.

Nevertheless, we made enough measurements on both 14- and 27-μm-thick waveguides (at ~10 different beam angles in the range $-20°$ to $+20°$) to draw some useful generalizations that both support the ray-tracing calculations and are explained (*a posteriori*) by them. In particular, we observed that for any absolute value of the incident angle θ, the energy throughput obtained when light is directed from a small but substantial angle below the waveguide surface ($-10° < \theta < -3°$) is substantially greater than the near-zero throughput obtained when the light is directed at a similar angle from above the waveguide surface plane, and typically up to ~20% greater than the throughput obtained when the synchrotron light is directed strictly on-axis ($\theta = 0°$). This empirical observation, which was very confusing at first, makes perfect sense in light of the subsequent ray-trace calculations shown in Fig. 4. This calculation demonstrates that negative values of θ in the range of $-3°$ to $-10°$ contribute far more to the total throughput of the waveguide than similar-magnitude positive angles, and slightly more than on-axis rays.

We also observed that the absorbance of a standard sample (e.g., the 3400 cm^{-1} peak for a 1-mm-diameter water droplet at the center of the waveguide sensing region) was only up to ~50% larger when the measuring synchrotron IR light impinged on the waveguide entrance face from 4°–10° below the waveguide plane than for light impinging on-axis. We had qualitatively expected that we would selectively excite high-angle modes at the sensing region of the waveguide by using light impinging off-axis onto the end face. However, the graphs in Fig. 4 contradict this expectation and instead support our empirical observation that it becomes only slightly easier to excite off-axis modes as the impinging angle is increased.

This explains why we found no input angle conditions for which we could get the water absorbance signal to approach that expected for light propagating at the critical angle. Figure 4 indicates that we might have been able to do this only if we had tightly focused the synchrotron beam at just the right entrance height (one of a few ~10-μm-high "sweet spots") on the entrance face of the cylinder–planar waveguide.

Oscillatory Signal on Absorbance Spectra Measured with Synchrotron Radiation. In general, the absorption intensity and band shape measured for the broad ν_{OH} band at 3400 cm^{-1} by using synchrotron radiation is similar to that measured by using a standard Globar™ source (Fig. 8). However, the spectra observed with the synchrotron show intense oscillatory interference patterns. As discussed previously for planar waveguides,[6] these oscillations arise from a fixed frequency separation between the allowed waveguide modes when the light is required to propagate between two planar surfaces with a well-defined propagation angle.

The strength of the interference phenomenon is greatly increased for the synchrotron-produced light due to its much greater spatial coherence (i.e., its ability to be simultaneously well-collimated and focused to a narrow beam diameter), relative to blackbody-generated irradiation. As a result, the entire synchrotron IR beam is propagated through the thinnest part of the waveguide at a

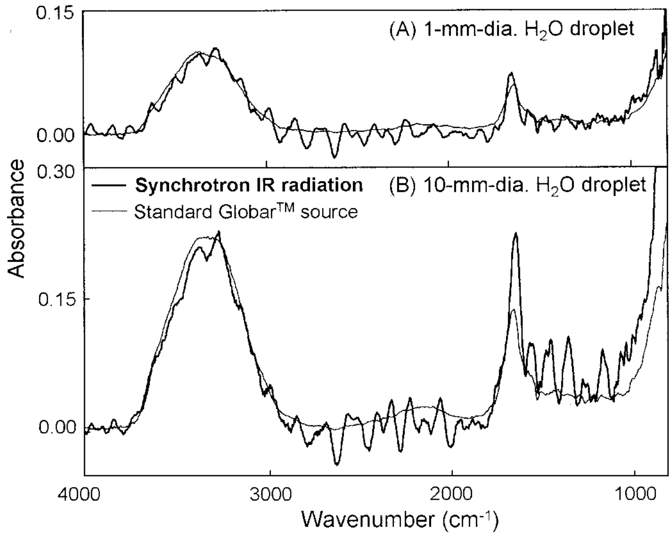

FIG. 8. Comparison of evanescent-wave absorbance spectra measured with a 14-μm-thick Ge waveguide, by using either synchrotron IR radiation (bold lines) or a standard blackbody (Globar®) source (thin lines). Samples were water droplets covering either (**A**) 1 mm or (**B**) 10 mm of the central part of the waveguide's sensing surface. These spectra were all collected with the in-compartment setup. The oscillatory interference pattern appears only with the synchrotron radiation, regardless of the waveguide thickness.

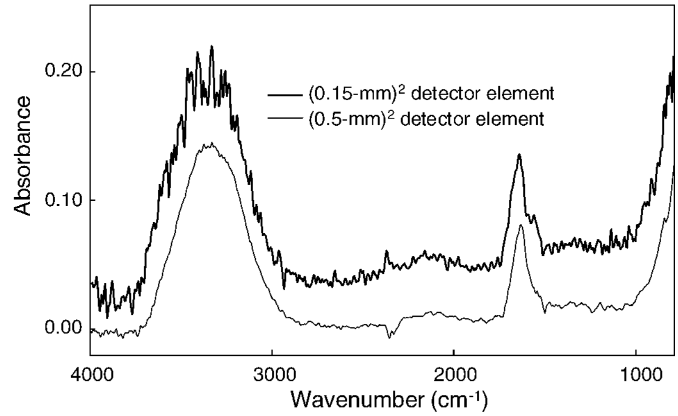

FIG. 9. Effect of size of the detector element on spectral signal-to-noise ratio observed for evanescent-wave absorbance measured from a 1-mm-diameter (~1 μL) water droplet. Both spectra were collected by using 5-min sample and background scans, with the same standard Globar® source and 14-μm-thick Ge waveguide, but with different lensed detectors carrying HgCdTe active elements either 0.50 or 0.15 mm on a side, as indicated.

single well-defined angle θ', which can be determined from the following formula giving the separation between allowed frequencies: $\Delta\nu = 1/(2nt \sin \theta')$, where n is the refractive index (4.0 for Ge) and t is the separation between the (approximately) planar surfaces. As discussed in the Experimental section, the thickness of each waveguide was previously measured using a variant of this equation, with IR light directed vertically through the waveguide from above, corresponding to $\theta' = 90°$. For the oscillating interference pattern in Fig. 8A, the calculated value of θ' corresponding to the measured $\Delta\nu = 125$ cm^{-1} was 45.6°. This is a reasonable value and indicates that the propagation of the synchrotron IR light through the Ge obeys well-understood equations.

In addition, the oscillating patterns observed with synchrotron light in Fig. 8 are very different from the much smoother baselines obtained with blackbody light, which propagates through the thinnest part of the tapered waveguide with a wide range of angles as shown in Figs. 2 and 4. It seems a bit strange at first glance that the oscillation of Fig. 8B is not as marked in the single-beam spectra from which it was calculated (e.g., Fig. 7). Presumably this is because in single-beam spectra measured with the waveguide, there is a superposition of different oscillation frequencies resulting from its tapered shape. This taper creates a wide range of separations between the two surfaces of the waveguide as the light propagates down its length.

In the case of absorbance measurements, however, the effects of the sample are concentrated in the region of minimum thickness, where the vast majority of the internal reflections occur (see Fig. 2). The main effect of the sample on the oscillation is simply a phase shift (without any frequency shift). The size of the phase shift is proportional to the number of internal reflections at the Ge–water interface. Thus, the oscillation frequency corresponding to the propagation angle at the minimum waveguide thickness is selected out of the superposition of oscillations corresponding to a range of greater thicknesses and shallower propagation angles. The superposition of the latter obscures the oscillations, which must nevertheless be present in the single-beam spectrum (Fig. 7).

An alternative approach that we additionally investigated for improving signal/noise ratio in our spectra was to use a smaller-area detector, since the manufacturer's spec sheet of the current detector indicated that the optical design of the 0.5-mm^2 detector element was optimized for collecting light from the output of an optical fiber somewhat larger than 1 mm^2. However, use of a different HgCdTe detector (FTIR-M16-0.10, Graseby Infrared), equipped with a 0.15-mm^2 detector element and the same immersion lens as the other detector, failed to produce absorbance spectra with a higher signal-to-noise ratio, at least when a Globar® source was used (Fig. 9). Furthermore, the use of this detector also resulted in the observation of a stronger oscillation pattern on the spectrum as compared to the larger immersion detector, similar to what was observed for the synchrotron-generated spectra (Fig. 8). From these observations, we conclude that the smaller detector area results in detection of only a selected portion of the IR throughput of the waveguide. The smaller detector appears to be functioning as a spatial filter, selectively observing a limited range of the optical modes that are transmitted through the waveguide. The particular vertical alignment of the detector determines which modes are detected.

CONCLUSION

Combining synchrotron-based IR spectroscopy with thin cylinder–planar Ge waveguides does not yet result in any overall improvement in the sensitivity of either technology for sensing small quantities of samples. However, there is clearly a throughput increase available with the synchrotron source, which is greater for thinner waveguides. Of course, for a sufficiently thick waveguide, a blackbody source can provide a greater total light energy flux than the synchrotron. The exact crossover thickness is dependent on the size of the detector element and focusing optics, but is typically somewhere in the range of 30–50 μm. Unfortunately, with waveguides in the range of 14–30 μm in thickness, the closer one approaches to single-angle operation (by using either a highly collimated source such as a synchrotron or a very small detector), the more deleterious is the oscillatory interference pattern that appears in the spectrum. This limits the application of synchrotron source light to the investigation of samples with such thin Ge waveguides. Thus, even for cylinder–planar waveguides as thin as 10 μm, a standard Globar™ source turns out to be more useful than the synchrotron, even though it cannot achieve quite such a high total energy throughput. However, for cylinder–planar waveguide sensors that are thinner than 10 μm or that have a non-cylindrical shape for their curved surface, the synchrotron may yet turn out to have important uses.

Furthermore, the ray-tracing computational method may potentially be used as a tool for optimizing the waveguide performance. The calculations suggest that the better performance (i.e., both for improved spectral quality and enhanced sensitivity) can be achieved by the cylinder–planar waveguides with a radius of curvature, at its bottom surface, in the range of 2000–3000 mm. This would consequently give rise to more powerful evanescent-wave sensors, particularly for microanalysis, in the near future.

ACKNOWLEDGMENTS

This research was supported by National Science Foundation (NSF) grant MCB-9722887 to M.S.B. and by additional funding from the Keck Center for Molecular Electronics at Syracuse University. Jitraporn Vongsvivut was supported by a fellowship from the Thailand Research Fund (TRF) via The Royal Golden Jubilee (RGJ) Program 3-C-CU-43-P-1 to Dr. Sanong Ekgasit (Chulalongkorn University, Bangkok, Thailand). We also would like to thank William F. Kutz of K & S Optics, who did most of the work involved in the fabrication process. In addition, it is a great pleasure to acknowledge the Center for Synchrotron Biosciences (U2B Beamline) at National Synchrotron Light Source (NSLS) in Brookhaven National Laboratory (BNL, Upton, Long Island) for financial and instrumental supports via NIH grant RR-01633, as well as help and technical support from Dr. Nebojsa Marinkovic at U2B beamline.

1. N. J. Harrick, *Internal Reflection Spectroscopy* (Harrick Scientific Corporation, Ossining, New York, 1979).
2. P. Niemela and J. Suhonen, Appl. Spectrosc. **55,** 1337 (2001).
3. D. S. Blair, L. W. Burgess, and A. M. Brodsky, Appl. Spectrosc. **49,** 1636 (1995).
4. D. S. Walker, W. M. Reichert, and C. J. Berry, Appl. Spectrosc. **46,** 1437 (1994).
5. M. S. Braiman and S. E. Plunkett, Appl. Spectrosc. **51,** 592 (1997).
6. S. E. Plunkett, S. Propst, and M. S. Braiman, Appl. Opt. **36,** 4055 (1997).
7. S. E. Plunkett, R. E. Jonas, and M. S. Braiman, Biophys. J. **73,** 2235 (1997).
8. J. J. Stone, M. S. Braiman, and S. E. Plunkett, Proc. SPIE-Int. Soc. Opt. Eng. **3105,** 371 (1997).
9. M. S. Braiman, S. E. Plunkett, and J. J. Stone, AIP Conf. Proc. **430,** 577 (1998).
10. M. S. Braiman and L.-Z. Mi, Proc. SPIE-Int. Soc. Opt. Eng. **3540,** 146 (1999).
11. S. V. Shilov, M. S. Braiman, and L.-Z. Mi, Proc. SPIE-Int. Soc. Opt. Eng. **3918,** 202 (2000).
12. J. Vongsvivut, S. V. Shilov, S. Ekgasit, and M. S. Braiman, Appl. Spectrosc. **56,** 1552 (2002).
13. N. J. Harrick, Appl. Opt. **10,** 2344 (1971).
14. *VUV Storage Ring Parameters as of December 2002,* retrieved March 1, 2003, from http://nslsweb.nsls.bnl.gov/nsls/org/AccPhys/vuv/vuv_parameters.pdf.
15. D. Marcuse, *Theory of Dielectric Optical Waveguides* (Academic Press, New York, 1991).